1-1995

Influence of Fabrication Technique on the Fiber Pushout Behavior in a Sapphire-Reinforced Nial Matrix Composite

R. Asthana
NASA Lewis Research Center

R. R. Bowman
NASA Lewis Research Center

Surendra N. Tewari
Cleveland State University, s.tewari@csuohio.edu

Publisher's Statement
Copyright 1995 ASM International. This paper was published in Metallurgical and Materials Transactions A: Physical Metallurgy and Materials Science, Vol. 26, Issue 1, pp. 209-223 and is made available as an electronic reprint with the permission of ASM International. One print or electronic copy may be made for personal use only. Systematic or multiple reproduction, distribution to multiple locations via electronic or other means, duplications of any material in this paper for a fee or for commercial purposes, or modification of the content of this paper are prohibited. Available on publisher's site at: http://www.springerlink.com/content/n010853112075397/.

Original Citation
Asthana, R., Tewari, S.N., & Bowman, R.R. (1995). Influence of Fabrication Technique on the Fiber Pushout Behavior in a Sapphire-Reinforced Nial Matrix Composite. Metallurgical and Materials Transactions A: Physical Metallurgy and Materials Science **26**, 209-223.

Repository Citation
Asthana, R.; Bowman, R. R.; and Tewari, Surendra N., "Influence of Fabrication Technique on the Fiber Pushout Behavior in a Sapphire-Reinforced Nial Matrix Composite" (1995). *Chemical & Biomedical Engineering Faculty Publications*. 25.
https://engagedscholarship.csuohio.edu/encbe_facpub/25

Influence of Fabrication Technique on the Fiber Pushout Behavior in a Sapphire-Reinforced NiAl Matrix Composite

R. ASTHANA, S.N. TEWARI, and R.R. BOWMAN

Directional solidification (DS) of "powder-cloth" (PC) processed sapphire-NiAl composites was carried out to examine the influence of fabrication technique on the fiber-matrix interfacial shear strength, measured using a fiber-pushout technique. The DS process replaced the fine, equiaxed NiAl grain structure of the PC composites with an oriented grain structure comprised of large columnar NiAl grains aligned parallel to the fiber axis, with fibers either completely engulfed within the NiAl grains or anchored at one to three grain boundaries. The load-displacement behavior during the pushout test exhibited an initial "pseudoelastic" response, followed by an "inelastic" response, and finally a "frictional" sliding response. The fiber-matrix interfacial shear strength and the fracture behavior during fiber pushout were investigated using an interrupted pushout test and fractography, as functions of specimen thickness (240 to 730 μm) and fabrication technique. The composites fabricated using the PC and the DS techniques had different matrix and interface structures and appreciably different interfacial shear strengths. In the DS composites, where the fiber-matrix interfaces were identical for all the fibers, the interfacial debond shear stresses were larger for the fibers embedded completely within the NiAl grains and smaller for the fibers anchored at a few grain boundaries. The matrix grain boundaries coincident on sapphire fibers were observed to be the preferred sites for crack formation and propagation. While the frictional sliding stress appeared to be independent of the fabrication technique, the interfacial debond shear stresses were larger for the DS composites compared to the PC composites. The study highlights the potential of the DS technique to grow single-crystal NiAl matrix composites reinforced with sapphire fibers, with fiber-matrix interfacial shear strength appreciably greater than that attainable by the current solid-state fabrication techniques.

I. INTRODUCTION

THE ordered intermetallic compound β-NiAl has excellent high-temperature oxidation resistance, relatively low density, a high melting point, and good thermal conductivity. However, its widespread use as a high-temperature structural material is limited because of its poor room-temperature ductility and toughness in polycrystalline form and its poor high-temperature strength. The current strategy to overcome these limitations involves two separate approaches. On the one hand, attempts are being made to improve the room-temperature toughness of monolithic NiAl by microalloying, by ductile phase toughening, and by single-crystal growth. On the other hand, the use of sapphire fibers as a reinforcement in the NiAl has been suggested to improve its high-temperature strength.[1,2] While a relatively weak fiber-matrix bond is desirable in brittle matrix composites from the fracture-resistance perspective, a strong bond is a prerequisite for high-temperature strengthening, where the fibers are the load-bearing constituents. In the case of β-NiAl, the use of sapphire fiber as a reinforcement material has been recommended[1,2] to improve the high-temperature strength by creating a strong fiber-matrix bond, rather than to improve the room-temperature toughness by creating a weak fiber-matrix

R. ASTHANA, National Research Council Associate, and R.R. BOWMAN, Engineer, are with the Materials Division, NASA Lewis Research Center, Cleveland, OH 44135. S.N. TEWARI, Professor of Chemical Engineering, is with Cleveland State University, Cleveland, OH 44115.

bond, as is usually done for brittle ceramic-matrix composites. Recent studies[3] also suggest that a strong sapphire-NiAl bond is required to withstand the radial tensile stresses that are generated during the heating portion of thermal cycling and to withstand interface shear near the fiber ends. A strong fiber-matrix bond, if properly optimized such that multiple matrix cracking conditions are satisfied, can increase the matrix cracking stress at room temperature.[3] A strong sapphire-NiAl interfacial bond is also required to achieve good cyclic oxidation resistance in the composite.[4]

One of the most common techniques of fabricating the sapphire-NiAl composites employs a powder cloth (PC) process or similar powder metallurgy (PM) techniques.[2] These processes produce a polycrystalline matrix material, thus precluding significant matrix ductility because of grain boundary (GB) incompatibilities.[5] In addition, the fiber-matrix interfacial shear strength in the sapphire-NiAl system is sensitive to the presence of binders used in the PC process,[1,4] resulting in a weak, frictional interfacial bond.

Recently, it was shown[6] on sapphire-NiAl composites with 0.5 vol pct fibers that casting and directional solidification (DS) have the potential to enhance the fiber-matrix interfacial shear strengths, measured using a fiber-pushout technique, compared to the current PM composites made using binders. Limited tests also showed that the low-volume-fraction DS composites had excellent thermal-fatigue resistance.[6] Preliminary results of fiber pushout on DS sapphire-NiAl composites showed less variability and consistently higher interfacial strengths than either as-cast or PC composites. It

was suggested that low variability and higher pushout strengths were primarily the result of fewer degrees of freedom for fiber location in the DS matrix. In the DS material, the fibers were either completely engulfed within grains or in contact with no more than one or two grain boundaries. This is in contrast to as-cast or PC composites, where the finer NiAl grain size invariably resulted in the termination of several grain boundaries at the fiber-matrix interface.

Previous studies[7-11] on fiber-pushout behavior in the sapphire-NiAl and other intermetallic matrix composites were focused mainly on the mechanics of the pushout process in a homogeneous matrix. In most of these studies, however, the pushout behavior was experimentally investigated in polycrystalline specimens in which the fiber diameter was appreciably larger than the average grain size of the matrix; as a result, several grain boundaries were coincident at the fiber-matrix interface. The fiber in these composites can, therefore, no longer be considered as residing in a homogeneous matrix, as required by the mechanistic models of fiber pushout.

The purpose of the present study was to further refine the DS process of fabricating sapphire-NiAl composites and investigate the effect of fabrication technique on the deformation and fracture behaviors of sapphire-NiAl composites during the fiber-pushout test. The role of matrix grain boundaries in the deformation behavior during pushout has been investigated by employing interrupted pushout testing and fractography of the PC and DS composites. In addition, the influence of the specimen thickness on the load-displacement response and fracture behavior has been examined.

II. EXPERIMENTAL PROCEDURE

The sapphire-NiAl fiber composites (fiber content of 28 vol pct) were fabricated using the PC process described in Reference 2. In this process, cloths of matrix alloy formed by mixing NiAl powder combined with organic binders are placed between plies made up of rows of alumina fibers and are diffusion bonded by application of high pressure at elevated temperatures. Single-crystal sapphire fibers, obtained from Saphikon, Inc. (Milford, CT) with an average diameter of 178 μm, were used as reinforcement. The PC (i.e., PM) composite plates (0.25 × 0.4 cm cross section) were used as feed material for DS. Directional solidification of the composite plates was carried out using a 30-kw RF generator coupled with a versatile crystal growth unit, which allows the same facility to grow single crystals in Bridgman, Czochralski, and float zone modes under vacuum or controlled atmosphere using a variety of translatory modes (e.g., seed rotation, crucible rotation, or zone translation). For the present set of experiments, DS was carried out by creating a float zone of 0.6- to 0.8-cm length using a copper concentrator (1.25-cm-diameter hole) and traversing this zone at a speed of 6.0 cm per hour along the length of the feed specimen. A 3 psi positive pressure of ultrahigh-purity argon was used during the solidification to suppress the loss of aluminum from the melt because of its high vapor pressure. The temperature of the zone was controlled to within ±6 K of the set temperature by a radiation pyrometer.

The fiber-matrix interfacial shear strengths of PC and PC + DS composite specimens were measured using a desktop fiber-pushout test apparatus[12,13] that records the time dependence of load during pushing (compressing) of a single-sapphire fiber embedded in the NiAl matrix by using a flat-bottomed punch of sintered tungsten carbide (150-μm diameter). The samples for pushout test were in the form of flat discs with a metallographic surface finish. Their thickness was varied from 240 to 730 μm to examine the influence of disc thickness on the fiber-pushout behavior. The discs were firmly glued to a steel sample holder (having 400-μm-wide grooves), taking care to align the fibers over the grooves so as to enable their unobstructed sliding during the pushout test. A motorized traverse mechanism allowed the sample to be moved toward the stationary punch at a rate of 0.82 μm s^{-1}. The load vs time data were recorded at 50-mS intervals for a period of 180 seconds or less and stored in computer files. In addition, the acoustic emission (AE) was also recorded during the fiber-pushout process. Generally, 5 to 15 tests were performed at each disc thickness for all samples. In order to relate the pushout behavior to microstructure in the vicinity of each tested fiber, the position of each fiber in the matrix was recorded with respect to its location at grain boundaries or grain interior prior to the test. The debonded surfaces of each fiber as well as the matrix surface in the region of displaced fiber on both the front (facing the tungsten carbide (WC) punch) and back faces of the PC and PC + DS specimens were also examined using optical microscopy (OM) and scanning electron microscopy SEM after interrupting the pushout test at various stages.

The sapphire fibers were extracted from the PC feed stock and PC + DS specimens for SEM examination by dissolving the matrix in a solution of 75 pct acetic acid, 23 pct nitric acid, and 2 pct hydrochloric acid. The NiAl matrix grain structure in the matrix was revealed by etching the polished samples with a solution of 25 pct acetic acid, 25 pct nitric acid, and 50 pct by volume water.

III. RESULTS

A. Optimization of the DS Process

Several runs were made to optimize the processing conditions for the DS of the feedstock composite specimens. The temperature of the melt was found to be the most important parameter from the standpoint of zone stability and fiber integrity. Figure 1 shows typical NiAl-sapphire specimens after DS at two different temperatures. The melt temperature for the specimen in Figure 1(a) was too high (2033 K) and resulted in an unstable melt zone (region "A"), variation in the specimen cross section, as well as fiber breakage. A DS temperature of 1993 K, however, was near optimum because no significant cross-sectional variation or fiber breakage was observed (Figure 1(b)). It is interesting to note that under the optimal growth conditions, it was possible to retain the initial shape of the feedstock specimen even after zone DS, as shown in Figure 1(c). The two views shown in this figure correspond to the two flat sides of the DS composite specimen with a rectangular cross section. During zone DS, the radio frequency
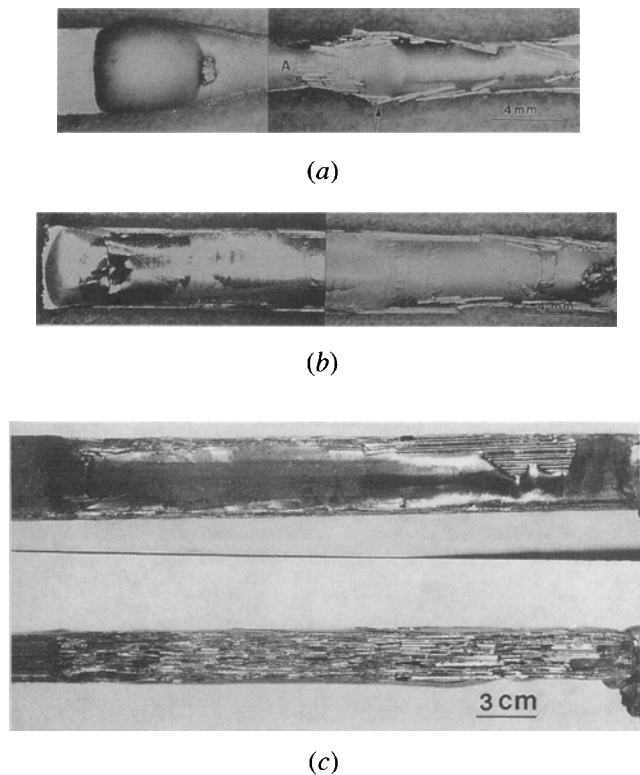
(a)

(b)

(c)

Fig. 1 — Typical views of PC sapphire-NiAl feedstock specimens after DS: (a) zone temperature (2033 K) is too high, resulting in an unstable floating zone and considerable fiber breakage; (b) near-optimum zone temperature (1993 K); and (c) front and side views of a DS specimen showing shape retention of the feedstock after zone DS.

(RF) current introduces an axisymmetric force field that tends to push the melt column toward the center of the concentrator. In addition, the eddy currents also introduce extensive thermal convection in the melt. The intensity of this convection is a maximum at the melt surface and decreases radially inward as a function of distance from the surface. Both the extent of the thermal convection and the tendency to create a cylindrical melt column are reduced in the presence of closely spaced sapphire fibers, which are held rigidly in place. It therefore becomes possible to retain a rectangular cross section during DS. However, at higher melt temperatures (larger RF currents), convection on the melt surface becomes more vigorous and the force pushing the melt column toward the center of the concentrator also increases, resulting in extensive fiber breakage, especially near the specimen surface. As the fibers at surface begin to break, local convection becomes more intense (only a skeleton of rigidly held and closely spaced fibers can suppress the convection), causing further breakage of the sapphire fibers (Figure 1(a)). The samples for subsequent characterization were, therefore, directionally solidified under the conditions depicted in Figures 1(b) and (c).

B. Microstructure

Figure 2 shows typical longitudinal (parallel to the growth direction) and transverse microstructures of PC

and PC + DS composites. The low-magnification view (Figure 2(a)) shows both the equiaxed PC feedstock portion (region A) and the DS portion (region B) of a typical specimen. This view is from a section through the central region of the specimen. For this sample, the zone was traversed along the direction marked by the arrow. Translation of the zone was stopped in the region marked C, resulting in a large shrinkage cavity there. Directional solidification produces grains that are aligned along the growth direction. Absence of significant fiber breakage resulting from DS is obvious in Figure 2(a). Figures 2(b) and (c), respectively, show the microstructure of the PC feed stock material parallel and perpendicular to the length of the sapphire fibers. The average grain size of the PC feed stock NiAl specimens was about 40 μm (Figure 2(b)), and several GBs were observed to terminate on the fiber surface (Figure 2(c)). Although intergranular voids (averaging about 10 to 20 μm in size) were occasionally observed in the PC material (marked "A" in (Figure 2(c)), in most instances, complete sintering appears to have occurred. Only the fibers located in the well-sintered regions were examined for their pushout behavior.

Figures 2(d) and (e), respectively, show the longitudinal and transverse microstructures of the PC + DS sample. In the PC + DS material, the grains are much larger, about 1000 μm (measured on the transverse section), and the fibers are either completely engulfed within the grain interior (GI), in which case the GBs have moved past the fibers, or are anchored by one to three GBs (Figure 2(d)) and (e)). However, the PC + DS material contained spherical gaseous microporosity in NiAl at the fiber-matrix interface, shown in Figure 2(f), where the sapphire fiber had been pulled out to reveal the three-dimensional distribution of this porosity. Because no such interfacial porosity was observed in DS sapphire-NiAl specimens made from a cast feedstock that did not contain any binders,[5] the porosities in the present DS specimens must have formed because of a reaction of binder residues in the PC material with oxygen in the melt during the DS process. In spite of the interfacial porosity, the interfacial shear strengths improved after DS compared to the original PC samples, as discussed in Section IV.

C. Extracted Fiber Surface

Figure 3 examines the sapphire fibers in the as-received condition and compares them with those extracted from the PC and PC + DS composites. The as-received sapphire-fiber surface was generally free of major defects, except for some surface asperities (Figure 3(a)), which were presumably produced because of the temperature and growth rate fluctuations during the melt growth of the fibers. The fibers also showed occasional longitudinal cracks, possibly as a result of handling (Figure 3(b)). The fibers extracted from the PC composite showed two major defects. One was a patchy residual debris adhering to the fiber surface (Figure 3(c)), and the other defect was GB ridges on the fiber surface, as marked by an arrow in Figure 3(d). These features, with an appearance similar to the well-known prior particle boundaries observed in hot isostatically pressed ("hiped") PM superalloys, may have
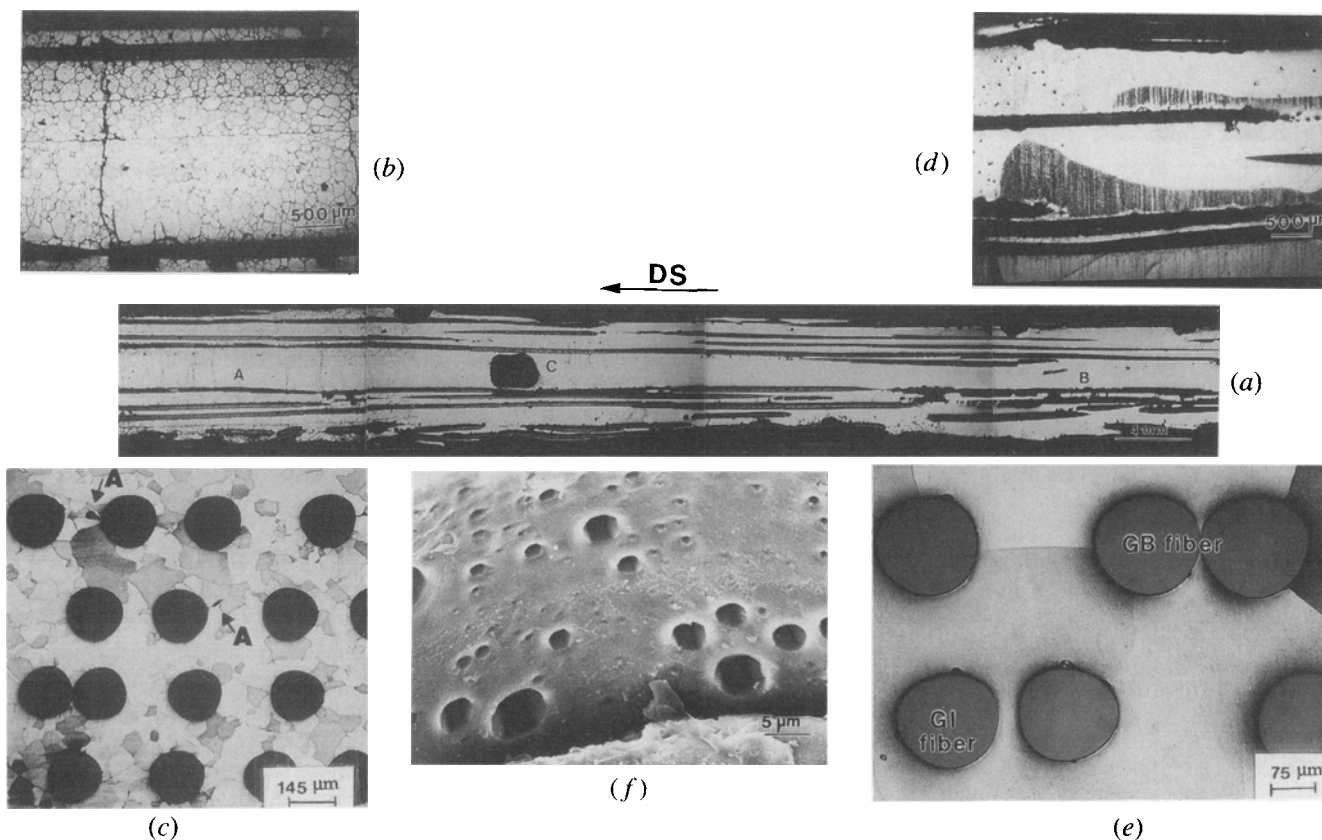
Fig. 2—Longitudinal and transverse microstructure (normal to the sapphire fibers) of sapphire-NiAl fiber composites: (a) low-magnification longitudinal view showing PC and DS regions (the arrow indicates the direction of zone traverse); (b) and (c) longitudinal and transverse views of PC region, respectively; (d) and (e) longitudinal and transverse views of DS regions, respectively (GB and GI indicate typical grain boundary and grain interior fibers); (f) SEM image of the NiAl matrix at a fiber-matrix interface after the fiber has been pulled out, showing gaseous porosity in PC + DS material.

formed by a reaction between the oxide layer on the NiAl powder surface with the sapphire fiber during sintering. Alternatively, the reaction between sapphire and NiAl may also take place, although thermodynamic calculations[14] rule out such a reaction below about 1583 K. Figure 3(e) shows a low-magnification view of several sapphire fibers extracted from the PC + DS composite. The dark spots (shown by an arrow in Figure 3(e)) are a crustlike reaction product layer adhering to the fiber surface (Figure 3(f)). This reaction product has not been identified in detail because it was only occasionally observed. Figure 3(g) represents the typical appearance of most of the fiber surface for the PC + DS composite. The gaseous porosity, described in relation to Figure 2(f), was also responsible for the circular features observed on the extracted fiber surface (Figure 3(g)). The notion that binder reactions cause the circular features on the fiber surface is supported by a previous work[6] in which sapphire fibers, extracted from a composite that was prepared by directionally solidifying a vacuum-cast sapphire-NiAl feed stock, did not show these defects. The surface of the fibers extracted from cast + DS composites shown in Figure 3(h) contained only the asperities that were present on the as-received fibers and showed neither the circular features resulting from the gaseous porosity nor the adherent reaction products observed in the DS composites prepared from the PC feedstock.

D. Fiber-Pushout Behavior

Figure 4 shows typical load-time plots and the accompanying AE from the fiber-pushout tests on PC and PC + DS samples. The notations PM, DS (GB), and DS (GI), respectively, will be used in the subsequent discussion to refer to fibers in powder-cloth processed material (which are in contact with numerous grain boundaries because of the small grain size), fibers in contact with GBs in PM + DS material (fiber in contact with at most three grain boundaries), and fibers located within the GI of PM + DS material (no fiber-GB contact). Figure 4(a) shows, schematically, the typical three-stage deformation process observed during the fiber-pushout tests: (1) an initial pseudoelastic region (A), where load was proportional to displacement up to a some stress τ_p; (2) an inelastic region (B) up to a maximum stress τ_m; followed by (3) a frictional region (C), where further fiber pushout was accomplished at a constant stress τ_f. The PM, DS (GB), and DS (GI) fibers in thick discs ($t/h > 0.75$, where t = disc thickness and h = groove width in the support, $h = 400 \mu m$) typically showed the preceding three-stage load-time (displacement) response (Figures 4(b) and (c)). The DS (GB) and PM fibers tend to show larger displacements during the second stage (region B), as compared to the DS (GI) fibers, and a somewhat discontinuous (stepped) load drop from the maximum value. The load drop beyond
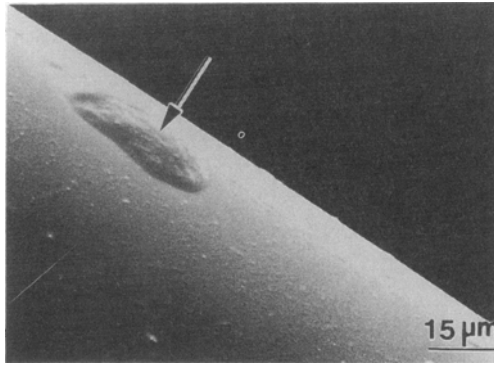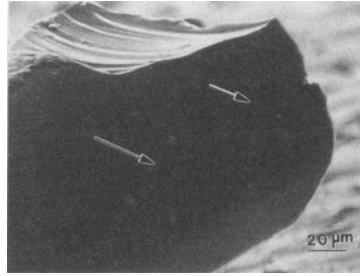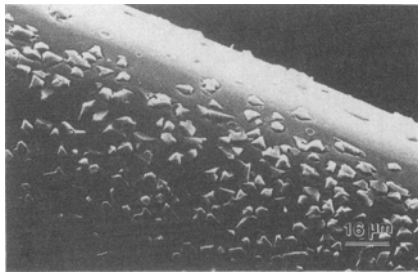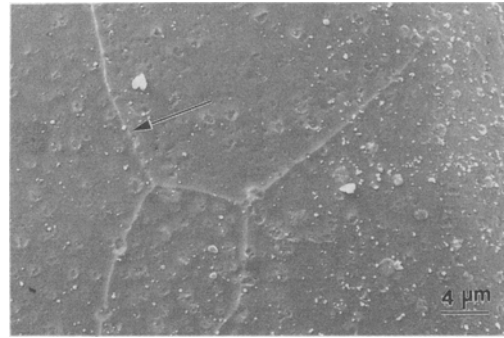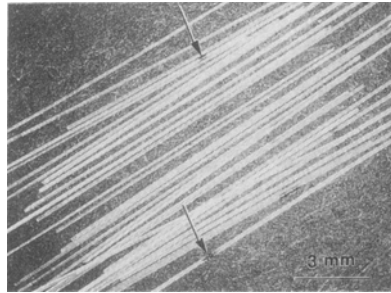
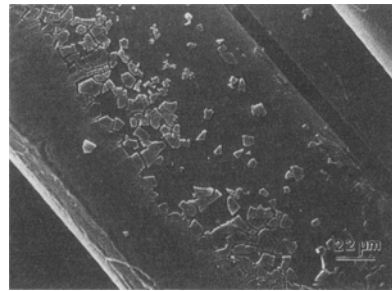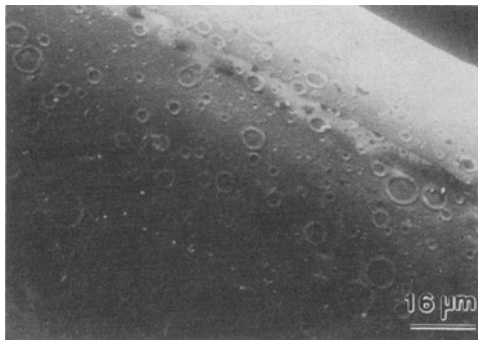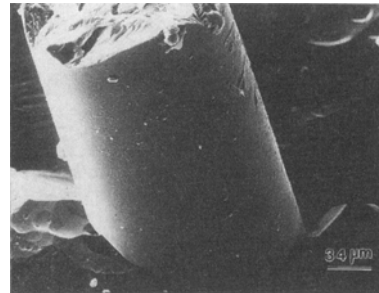Fig. 3—Surface appearance (SEM images) of as received sapphire fibers and fibers extracted from composites: (*a*) and (*b*) as-received fiber; (*c*) and (*d*) PC processed (PM); (*e*) low-magnification view of fibers extracted from PC + DS composite; (*f*) and (*g*) PC + DS; and (*h*) cast + DS.[16]
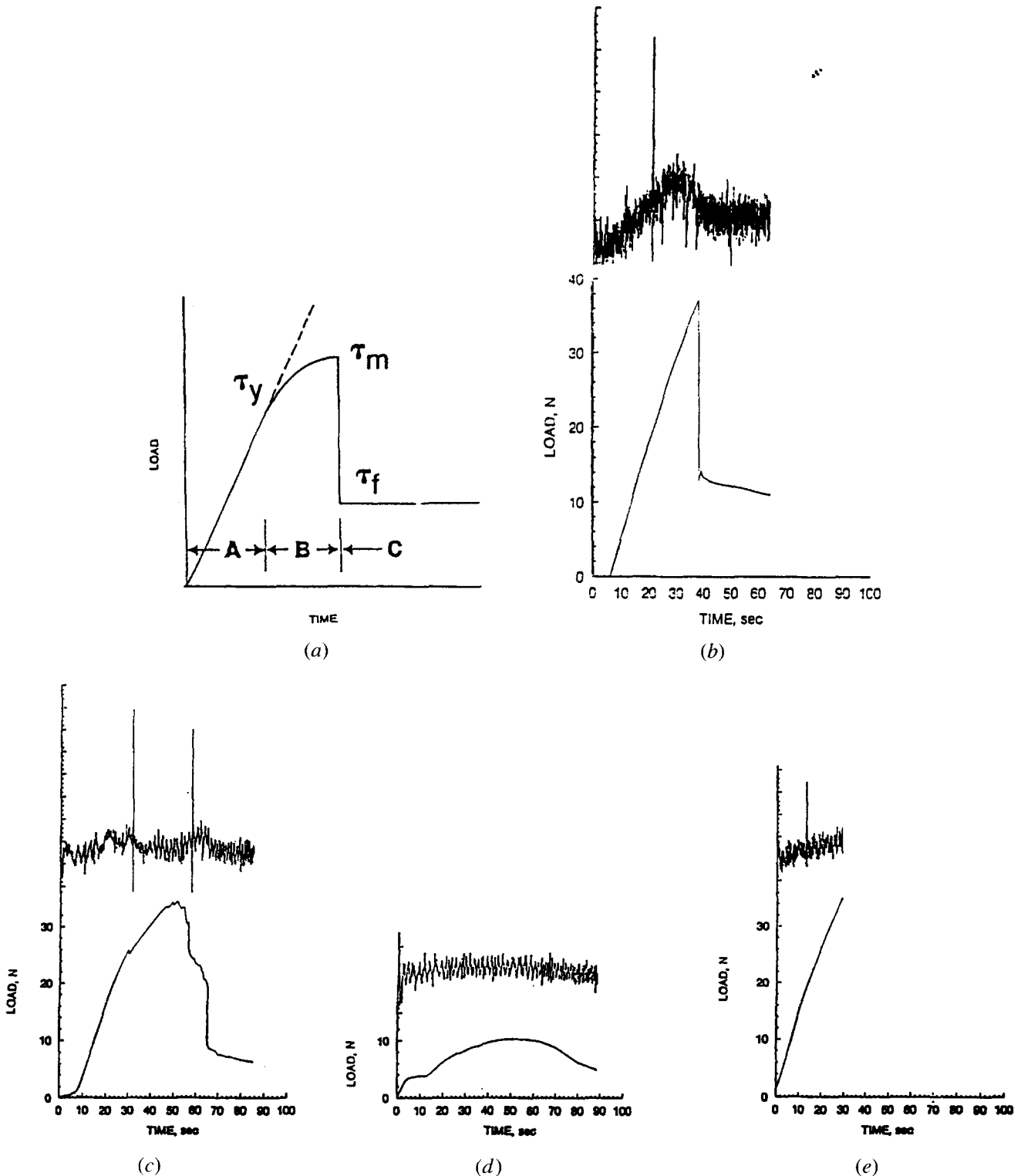
Fig. 4—Load-time and AE data from the fiber-pushout test on sapphire-NiAl composites. The shear stresses corresponding to transition between regions A and B and between regions B and C are defined as the proportional shear stress, τ_p, and the maximum shear stress, τ_m, respectively. (a) Schematic load-time plot for thick ($t/h > 0.75$) specimens. Region A is the linear (pseudoelastic) response, region B is the inelastic response, and region C is the constant (friction) load regime. Typical responses for thick ($t/h > 0.75$) specimens: (b) DS (GI) and (c) DS (GB) and PM specimens are compared to the response for (d) thin ($t/h < 0.75$) PM specimens. (e) Load-time plot for a fiber in a thick PC + DS specimen ($t/h > 1.3$) in which complete fiber pushout could not be achieved because of load limitations of the instrument.

the maximum in region B invariably occurred in a single sharp step for DS (GI) fibers.

The load-displacement response of relatively thin ($t/h \leq 0.75$) discs was generally very different from that of the thick discs. The PM and DS (GB) fibers in thin discs (Figure 4(d)) showed a continuous increase in load to a maximum, followed by a gradual decrease to a constant value with no sharp drop in load. On the other hand, the load-time response of DS (GI) fibers in thin discs was similar to that of thick discs and showed the three-stage deformation behavior described previously. Although all fibers tested in PC specimens could be pushed out for all the disc thicknesses (240 to 700 μm), the maximum permissible load (35 to 40 N) during the test was sometimes insufficient to push the fibers in thicker ($t/h > 1.3$) PC + DS specimens. The load-time response in such cases consisted only of regions A and B (Figure 4(e)).

Generally, a strong acoustic signal was detected at the "proportional limit" (the transition point between regions A and B in Figure 4(a)); however, the intensity of the signal appeared to be largely independent of disc thickness for both PC and PC + DS samples, as shown in Figure 5. The lines in this figure indicate the standard deviation in the acoustic signal-to-noise ratio.

The pushout behavior of sapphire-NiAl composites will be described in terms of the following parameters: proportional shear stress (τ_p), corresponding to the load at the transition point between regions A and B in Figure 4(a); maximum shear stress (τ_m), corresponding to the maximum load at the transition between regions B and C; frictional shear stress (τ_f) in the constant load region C, and the extent of pseudoelastic deformation. The τ_p, τ_m, and τ_f values are obtained by dividing the corresponding load values by the interfacial contact area
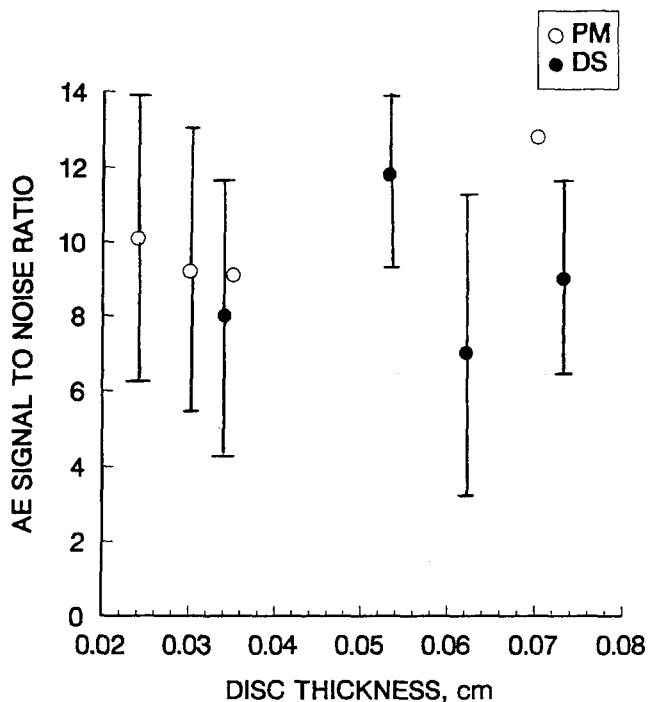

Fig. 5—AE signal-to-noise ratio at the proportional shear stress for PM and PM + DS specimens as a function of disc thickness.

($\pi D t$), where D is fiber diameter and t is the disc thickness (which is also the embedded length of the fiber). The average values of τ_p, τ_m, τ_f, and their standard deviations have been compiled in Table I. Because interfacial shear strength measurements were made over a relatively wide range of disc thickness (240 to 730 μm), the τ_p, τ_m, and τ_f values in Table I have been presented separately for the thin specimens ($t/h \leq 0.75$) and thick specimens ($t/h > 0.75$).

1. Proportional shear stress

Figure 6 shows plots of the proportional shear stress (τ_p) for thick (Figure 6(a)) and thin (Figure 6(b)) PM, DS (GB), and DS (GI) fibers, while Table I summarizes the mean values of proportional shear stresses, as well as the standard deviation. First, the behavior of the thick specimens will be compared with the thin ones. For the DS (GI) fibers, the mean τ_p value for the thin ($t/h \leq 0.75$) discs (77 ± 24 MPa) is smaller than that for the thick discs (97 ± 39 MPa). However, for the PM fibers, the mean τ_p values of the thin and thick discs are nearly equivalent (within ±3 MPa) (Table I). Figure 6 also shows that the PM material has a significantly smaller τ_p than the DS (GB) and DS (GI) fibers for both thin and thick specimens. Because the proportional shear stress (τ_p) is generally taken[11] to represent the initial debond shear stress, Figure 6 suggests that the interfacial bonds are the strongest in DS (GI) material and weakest in the PM material. This is illustrated by the mean τ_p values for the thick specimens, which are 30 ± 14, 82 ± 32, and 97 ± 39 MPa, for PM, DS (GB), and DS (GI), respectively (Table I).

2. Maximum shear stress

Figure 7 shows the maximum shear stress (τ_m), for thick and thin PM, DS (GB), and DS (GI) samples, and Table I summarizes the mean values of τ_m, as well as the standard deviation. The numbers in parentheses adjacent to mean τ_m in this table refer to the numbers of fibers that could not be pushed within the load capacity of the instrument. The PM fibers could all be pushed out irrespective of their disc thickness, whereas the maximum disc thickness in which the DS (GB) fibers could be pushed was about 500 μm, compared to about 350 μm for the DS (GI) specimens. This indicates that the maximum pushout strengths would be in the order

Table I. The Mean Values of Proportional Shear Stress, τ_p, Maximum Shear Stress, τ_p, and Frictional Shear Stress, τ_f, for Thick ($t/h > 0.75$) and Thin ($t/h \leq 0.75$) Test Specimens*

	τ_p (MPa)	τ_m (MPa)	τ_f (MPa)
PM ($t/h \leq 0.75$)	27 ± 13	30 ± 16	20 ± 13
($t/h > 0.75$)	30 ± 14	42 ± 21	22 ± 9
DS (GB) ($t/h \leq 0.75$)	80 ± 47	137 ± 79	42 ± 23
($t/h > 0.75$)	82 ± 32	>89 ± 40 (33)	28 ± 15
DS (GI) ($t/h \leq 0.75$)	77 ± 24	151 ± 59	19 ± 9
($t/h > 0.75$)	97 ± 39	>123 ± 32 (4)	32 ± 11
CAST + DS + TC[6]	142 ± 37	>180	10

*Numbers in parentheses against τ_m values indicate the numbers of fibers that could not be pushed within the loading capacity of the instrument.
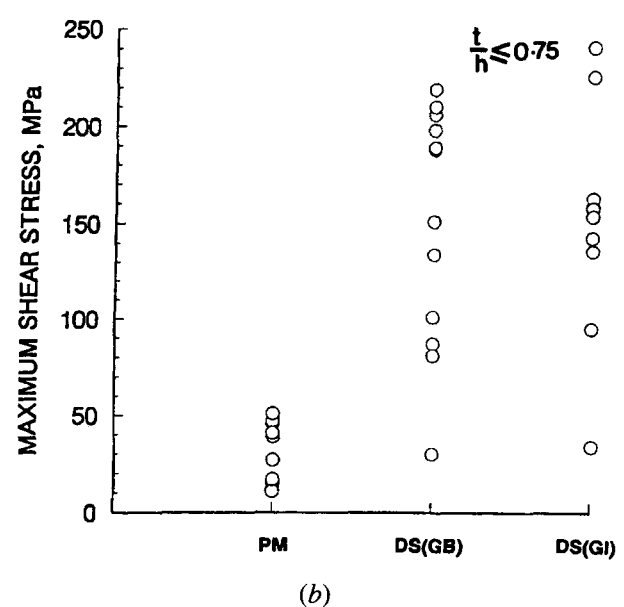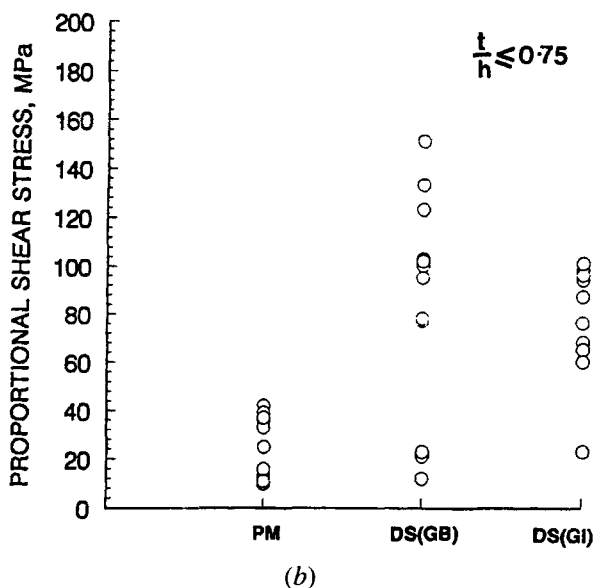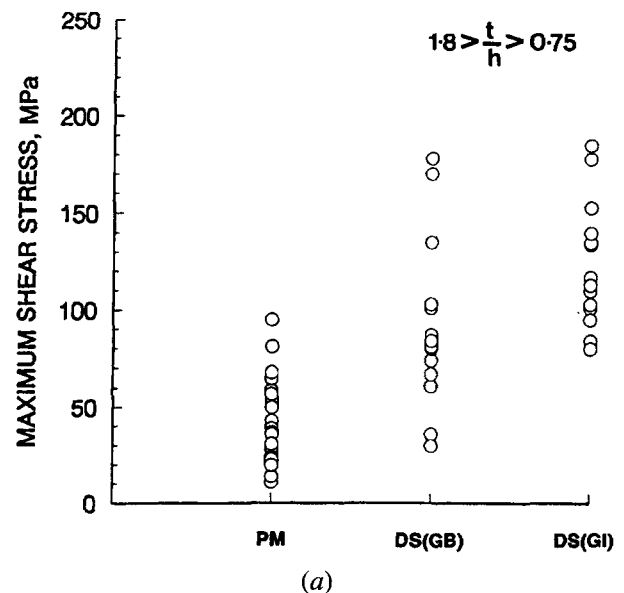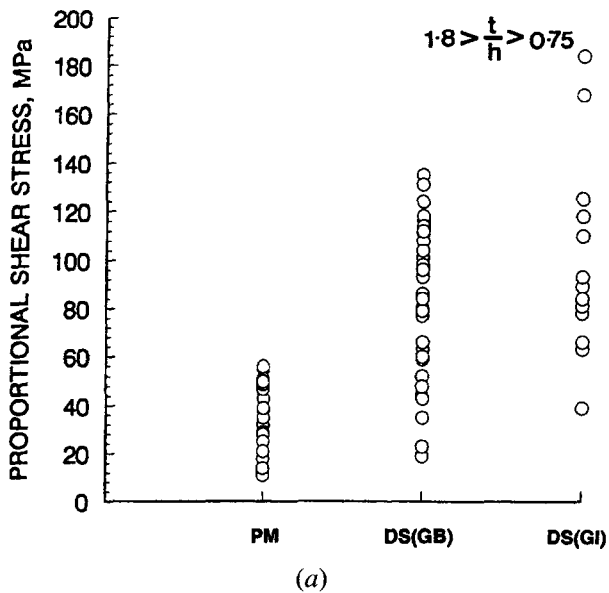
Fig. 6—Experimental values of the proportional shear stress, τ_p, for (1) PM, (2) DS (GB), and (3) DS (GI) fibers in (a) thick ($t/h > 0.75$) and (b) thin ($t/h < 0.75$) specimens.

Fig. 7—Experimental values of the maximum shear stress, τ_m, for (1) PM, (2) DS (GB), and (3) DS (GI) fibers in (a) thick ($t/h > 0.75$), and (b) thin ($t/h \leq 0.75$) specimens.

of DS (GI) > DS (GB) > PM, similar to the variation of τ_p, seen in Figure 6. Because τ_m values for the unpushed DS (GB) and DS (GI) fibers could not be obtained, the mean τ_m values listed in Table I represent a lower limit, as represented by this symbol: >. No correlation was observed between τ_m and the disc thickness for the PM, DS (GB), and DS (GI) samples. The mean τ_m values for thick samples, considering only the pushed-out fibers were PM = 42 ± 21 MPa, DS (GB) = 89 ± 40 MPa, and DS (GI) = 123 ± 32 MPa.

3. Frictional shear stress

Figure 8 plots frictional shear stress (τ_f) for both thick and thin PC and PC + DS samples. The mean values of the frictional shear stress together with the standard deviation are listed in Table I. The frictional shear stress was calculated at an arbitrary displacement of 10 μm beyond the maximum shear stress, regardless of whether

a sharp-load-drop type behavior was observed or not. The average values of frictional shear stress for thin PM, DS (GB), and DS (GI) samples were 20 ± 13, 42 ± 23, and 19 ± 9 MPa, respectively. The average τ_f values for thick PM, DS (GB), and DS (GI) specimens were 22 ± 9, 28 ± 15, and 32 ± 11, MPa, respectively. The relative independence of the frictional shear stress to microstructure in the case of thick sapphire-NiAl composites suggests that once the fiber is completely debonded, the sliding of the fiber is not affected by disc thickness, processing history, or the matrix structure. In contrast to the present values of frictional shear stress during forward sliding, the frictional shear stress during the reverse pushout in a PM sapphire-NiAl composite has been reported to be 45 ± 11 MPa.[7] The frictional shear stress during reverse pushout would be expected to be lower

than that during the forward pushout, because the asperities on the fiber surface will remain in registry with the grooves formed during the forward motion. The reason for the inconsistency between our values of the forward frictional stress and those reported during the reverse pushout is not clear. Although no details of the PM fabrication process (whether binders were used) were available in Reference 9, the interfacial shear strengths reported (87 ± 37 MPa) are comparable to the values reported by others for PM samples made using binders.[11]

4. Pseudoelastic displacement

The displacement in the "pseudoelastic" region of the load-displacement plot was measured because it gives an estimate of the relative magnitude of elastic bending of
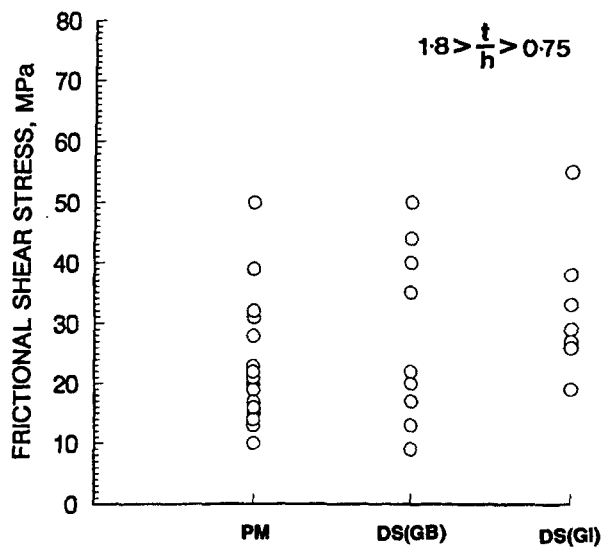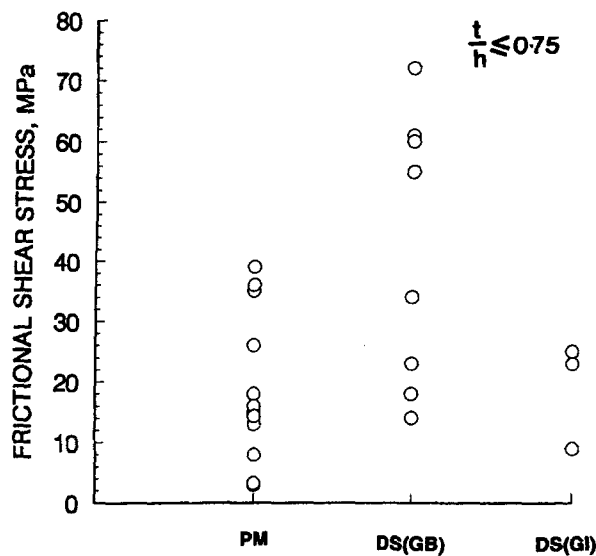
the test specimen during the fiber-pushout test. It is expected that in the initial linear (pseudoelastic) region of the load vs displacement plots (A in Figure 4 (a)), the experimentally observed displacement will also include the effects of specimen bending, especially for the thin discs. This would cause a decrease in the slope of the load vs displacement plots in region A, compared to a case in which no specimen bending occurred. In order to quantitatively represent this effect, the experimentally measured displacements at a load of (1.37 N) have been plotted as a function of disc thickness in Figure 9. This value of load represents the smallest observed load corresponding to a proportional limit in the present set of experiments. The PM fibers show a distinct disc-thickness dependence, for which the displacements are minimized only for disc thicknesses >300 μm. In addition, for the PM material, the scatter for the thinner discs is much larger as compared to the thick ones. The DS (GB) fibers (open circles) appear to show some disc-thickness dependence, whereas the DS (GI) fibers do not show any disc-thickness dependence. The pseudoelastic displacement for DS (GB) fibers is less than the PM fibers at small thicknesses but is approximately the same as PM samples at larger thicknesses ($t/h > 0.75$). The DS (GI) fibers generally showed the least displacements for all the disc thicknesses examined in this study. As indicated by the filled square symbol in Figure 9, the displacement value for the PM sapphire-NiAl composites reported in another study (extracted from Figure 7 of Reference 11) compares well with the behavior observed in the present study. It is also interesting to note that for a 500-μm-thick PM sapphire-NiAl composite disc, the total displacement to failure of 6.3 μm reported in Figure 7 of Reference 10 compares well with the total

Fig. 8—Experimental measurements of the frictional shear stress, τ_f, for (1) PM, (2) DS (GB), and (3) DS (GI) fibers in (a) thick ($t/h >$ 0.75) and (b) thin ($t/h \leq$ 0.75) specimens. The frictional shear stress has been defined at the load corresponding to a displacement of 10 μm beyond the maximum loads in the pushout profiles.
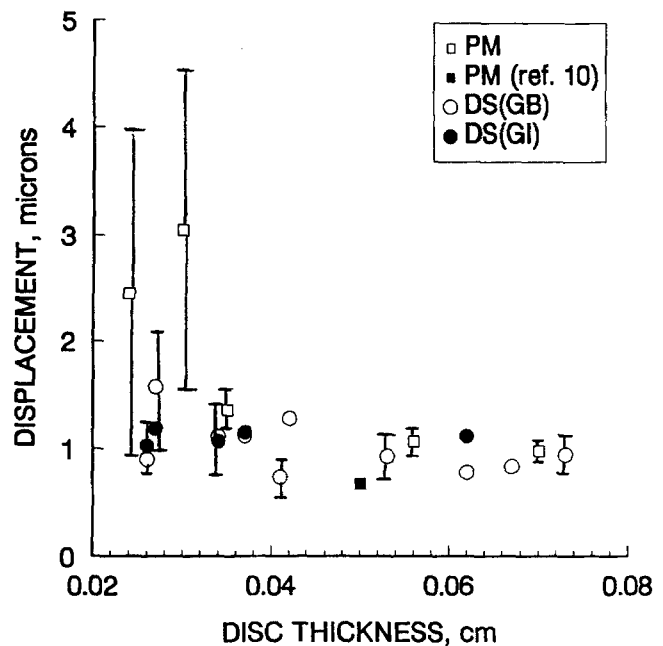
Fig. 9—The extent of pseudoelastic displacement vs disc thickness at 1.37 N load (smallest load corresponding to the proportional limit in the present set of experiments). Computations are made for each disc thickness based on the mean values of the slopes of load vs displacement profiles for that thickness.

displacement of 6 ± 2 μm for the 560-μm-thick discs of the present PM specimens.

E. *Fracture Behavior*

1. *PC processed composites*

Figure 10 summarizes the fracture behavior of PM (PC) specimens during the fiber-pushout test interrupted at τ_p and τ_m on the load-displacement curves. The thin PM specimens showed formation of fine radial cracks in the matrix on the front face (facing the tungsten carbide punch) (Figure 10(a)) and limited decohesion of the fiber-matrix interface as well as radial cracks on the back face (Figure 10(b)) when the applied stress was slightly greater than τ_p. When the test was interrupted at $\tau \geq \tau_m$, the thin PM specimens showed extensive cracking on both the front (Figure 10(c)) and back (Figure 10(d)) faces. For thick ($t/h > 0.75$) PM specimens, no interfacial damage was observed either on the front (Figure 10(e)) or back (Figure 10(f)) face when the test was interrupted at $\tau \geq \tau_p$. However, when the test was

interrupted at $\tau \geq \tau_m$, both the front (Figure 10(g)) and back (Figure 10(h)) faces of thick specimens showed extensive interfacial cracking along GBs that were coincident on the fiber. There was also evidence of NiAl grains being lifted above the flat back face of the specimen as the fiber debonded and slid at $\tau \geq \tau_m$ (Figure 10(h)).

2. *DS composites*

Figure 11 summarizes the fracture behavior observed when the pushout test was interrupted at τ_p and τ_m. Note that the disc thicknesses (270 to 730 μm) are much larger than the total fiber displacement during pushout at $\tau > \tau_m$. For the DS (GB) and DS (GI) fibers in both thick and thin discs, no visible interfacial cracking was present on the front (Figure 11(a)) and back (Figure 11(b)) faces when $\tau \geq \tau_p$. However, it should be noted that acoustics signals were generally observed to occur in the vicinity of τ_p (Figure 4). This suggests that some micromechanical events, possibly too weak to leave behind any gross microstructural manifestations detectable at optical magnifications, do occur at the fiber-matrix interface at τ_p.

(*a*)

(*b*)

(*c*)

(*d*)

Fig. 10—Fracture surfaces of PC specimens at τ_p and τ_m in the interrupted pushout tests. (*a*) through (*d*) are for thin ($t/h \leq 0.75$) disc, and (*e*) through (*h*) are for thick ($t/h > 0.75$) discs. (*a*) and (*b*) are front- and back-face views, respectively, at τ_p; (*c*) and (*d*) are front- and back-face views, respectively, at τ_m; (*e*) and (*f*) are front- and back-face views, respectively, at τ_p, and (*g*) and (*h*) are front- and back-face views, respectively, at τ_m.
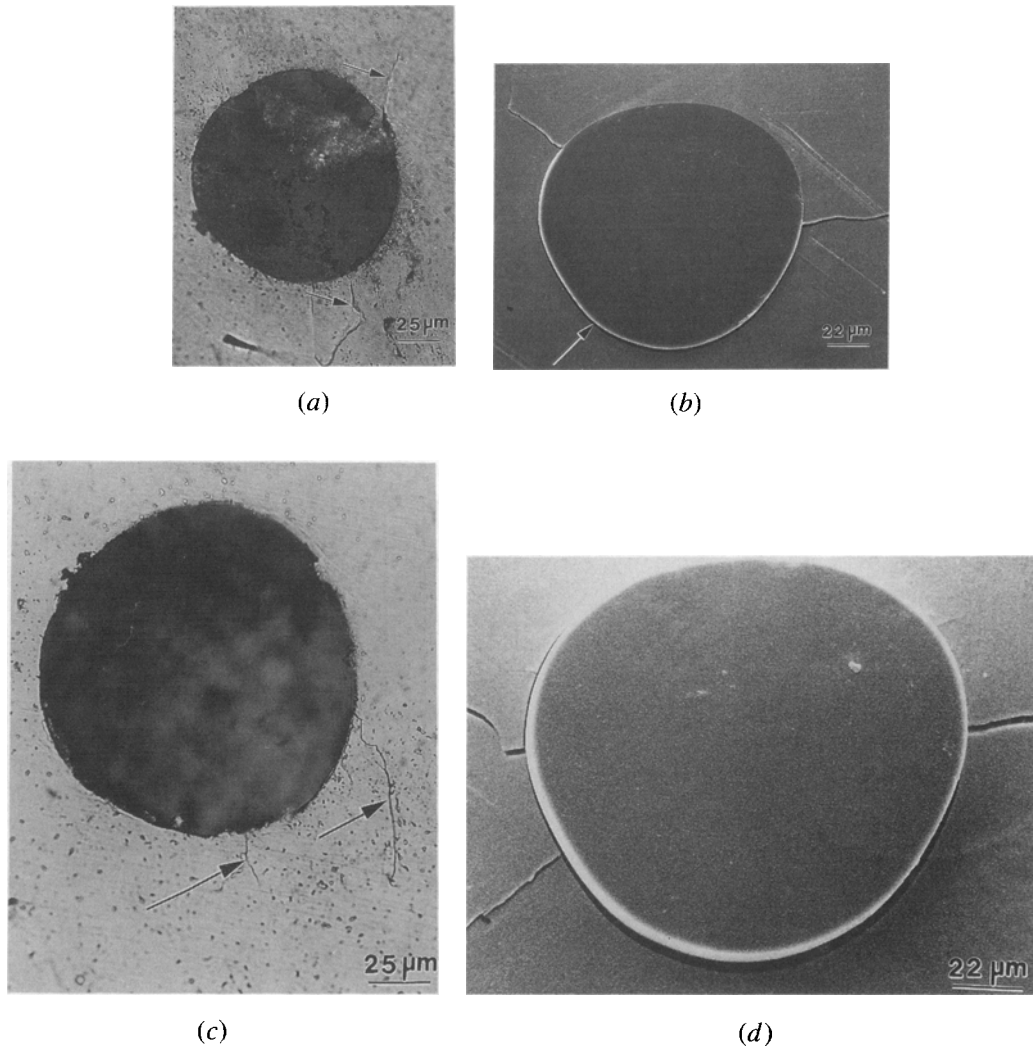
(e)

(f)

(g)

(h)

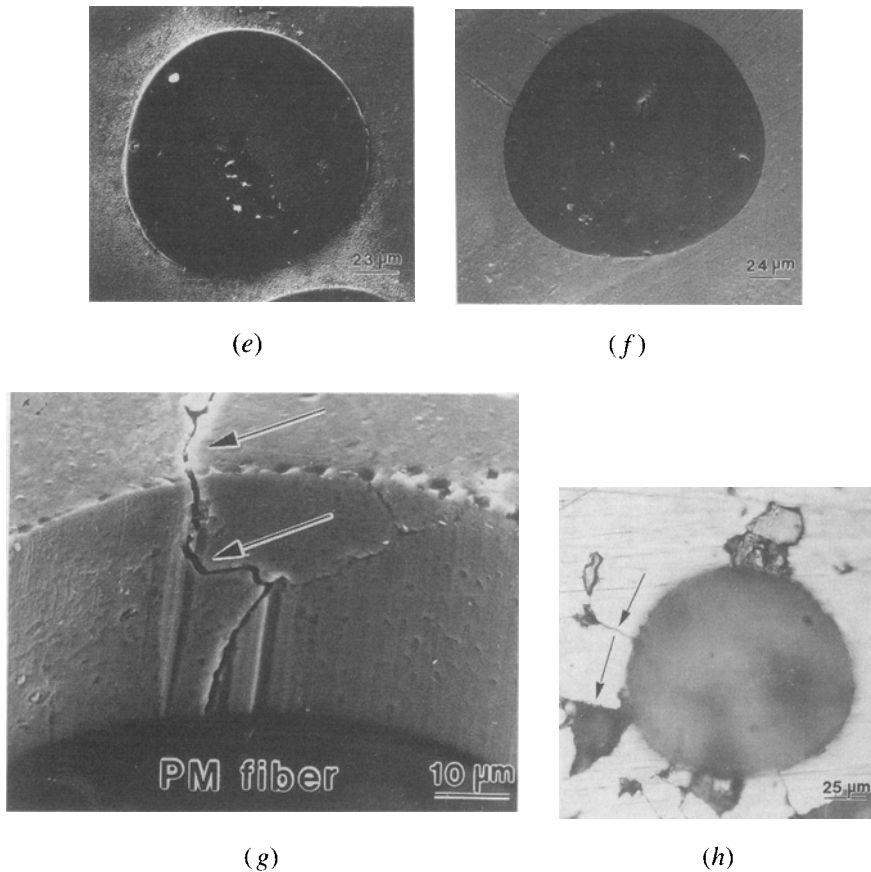Fig. 10 Cont. — Fracture surfaces of PC specimens at τ_p and τ_m in the interrupted pushout tests. (a) through (d) are for thin ($t/h \leq 0.75$) disc, and (e) through (h) are for thick ($t/h > 0.75$) discs. (a) and (b) are front- and back-face views, respectively, at τ_p; (c) and (d) are front- and back-face views, respectively, at τ_m; (e) and (f) are front- and back-face views, respectively, at τ_p, and (g) and (h) are front- and back-face views, respectively, at τ_m.

When the pushout test was interrupted just after τ_m (Figure 11(c)), the front faces of DS (GB) fibers in both thick and thin specimens showed crack formation at the GBs that were coincident on the fiber surface. The back faces of these fibers showed both GB cracking and circumferential decohesion along part of the fiber-matrix interface (Figure 11(d)). Thus, the GBs that are coincident on the fiber-matrix interfaces in DS (GB) specimens appear to be preferred sites for crack nucleation and growth. This would explain the lower values of τ_p and τ_m for the DS (GB) fibers as compared to the DS (GI) fibers (Table I).

The SEM examination of the DS (GI) fibers when the test was interrupted at τ_m but before large-scale fiber sliding commenced showed no interfacial damage on the front face (Figure 11(e)), but it did show partial fiber-matrix debonding together with fine radial cracks on the back face (Figure 11(f)). It appears that for the DS (GI) fibers, the fiber-matrix decohesion begins on the back face in the inelastic regime on the load vs displacement curve. The radial cracks shown in Figure 11(f) are then formed when the circumferential crack gets deflected into the matrix during its growth.

Finally, when the pushout test was interrupted in the frictional regime (after large-scale fiber sliding had occurred), the DS (GB) fibers in both thick and thin specimens showed interfacial cracking on the front and back

faces (Figures 11(g) and (h), respectively). On the other hand, the DS (GI) fibers still did not have any visible front-face damage (Figure 11(i)), and only back-face interfacial cracks (Figure 11(j)) were observed. Similar back-face cracking was also observed in the sapphire-NiAl composites made by casting and DS techniques.[6] The SEM views also show evidence of plastic grooving of the NiAl matrix, which appears as long streaks on the matrix surface parallel to the pushout direction in Figure 11(i). Such plastic grooving of the matrix may be caused by fiber asperities and wear debris generated during postdebond sliding of the fiber relative to the matrix. The gaseous porosity at the fiber-matrix interface due to the binder burnout and gas release during DS, mentioned previously, are also evident in Figures 11(g) and (i).

IV. DISCUSSION

The results of this study show that the deformation processes that occur during fiber pushout are influenced by the nature of the fiber-matrix interface and the matrix structure in the vicinity of the fiber-matrix interface, both of which are influenced by the fabrication technique. In addition, there is strong evidence that the failure mechanism during pushout can be dictated by the test
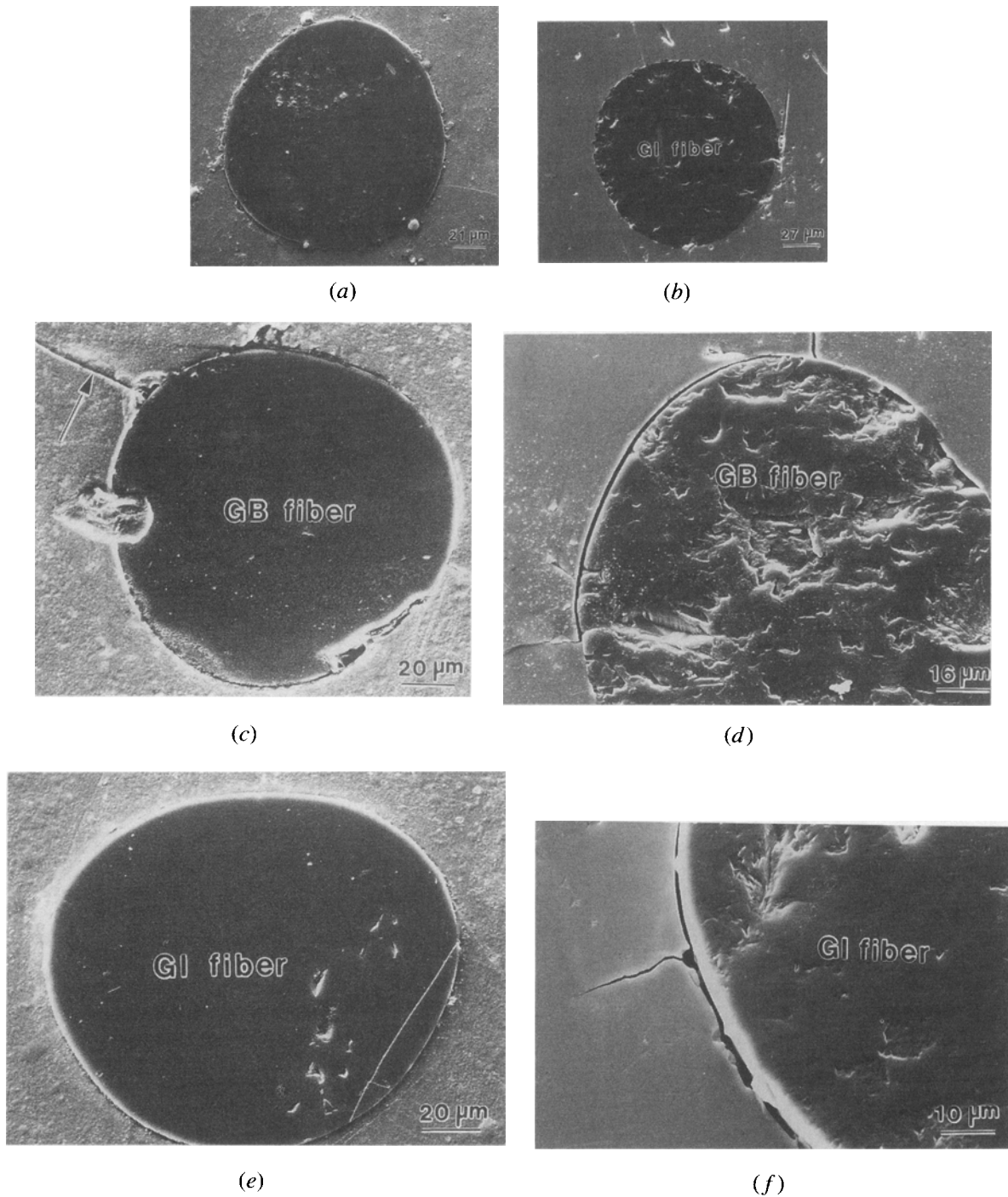
(a)   (b)

(c)   (d)

(e)   (f)

Fig. 11—Fracture surfaces of PC + DS specimens at τ_p and τ_m in the interrupted pushout tests. (No difference between thick and thin discs was observed for the PC + DS specimens.) (a) Front-face and (b) back-face views at τ_p for DS (GB) and DS (GI) fibers; (c) front-face and (d) back-face views at τ_m for DS (GB) fiber; (e) front-face and (f) back-face views at τ_m for DS (GI) fibers; (g) front-face and (h) back-face views at $\tau > \tau_m$ (friction regime) for DS (GB) fibers, and (i) front-face and (j) back-face views at $\tau > \tau_m$ for DS (GI) fibers.

conditions (e.g., the t/h ratio) rather than by the intrinsic behavior of the composite, especially for thin specimens. Recent finite element modeling[11] studies of fiber pushout suggest that for test geometries where the ratio of specimen thickness (t) to support hole diameter (h) was less than 2, the interfacial stresses were not independent of specimen geometry and not constant over the fiber length. It was observed that in the sapphire-NiAl composite, the combined thermal and mechanical stress distributions result in a large radial-stress component at the specimen back face, which can initiate cracks at the specimen back face and permit their growth

(g)   (h)
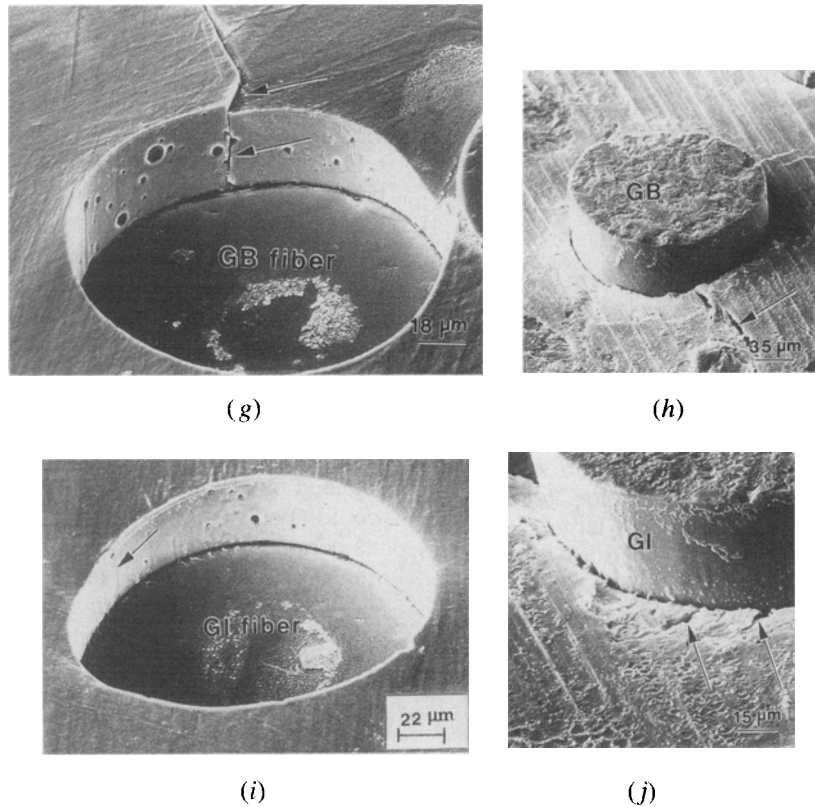

(i)   (j)

Fig. 11 Cont.—Fracture surfaces of PC + DS specimens at τ_p and τ_m in the interrupted pushout tests. (No difference between thick and thin discs was observed for the PC + DS specimens.) (a) Front-face and (b) back-face views at τ_p for DS (GB) and DS (GI) fibers; (c) front-face and (d) back-face views at τ_m for DS (GB) fiber; (e) front-face and (f) back-face views at τ_m for DS (GI) fibers; (g) front-face and (h) back-face views at $\tau > \tau_m$ (friction regime) for DS (GB) fibers, and (i) front-face and (j) back-face views at $\tau > \tau_m$ for DS (GI) fibers.

along the interface. The evidence of such back-face cracks during fiber pushout also can be seen in the fractographs of Figures 10 and 11.

A. Pushout Behavior: Interfacial Shear Strength

In the present study, the NiAl GBs coincident on the sapphire-fiber surface were observed not only to be the preferred sites for nucleation of the cracks but also to provide an easy path for the crack growth. The sapphire fibers in the PC material, because of a small grain size (40 μm), had the maximum number of such GBs, resulting in the easy nucleation of such cracks and the lowest τ_p values (27 ± 13 MPa). The fibers in the DS materials (grain size of 1000 μm), with a smaller number of such GBs, showed larger τ_p values (82 ± 32 MPa). The fibers that were located in the interior of DS NiAl grains showed the largest τ_p values (97 ± 39 MPa). Within the limitations of the pushout test, these values would, therefore, be expected to represent the "inherent" sapphire-NiAl interfacial shear strength. It is also worth noting that sapphire fibers in the DS samples made from a cast feedstock,[6] with an interface free of microvoids, showed the highest τ_p values (142 ± 37 MPa). It is therefore conceivable that the presence of gaseous microporosity in the PC + DS composites used in the present study assisted interfacial debonding. Thus, besides the matrix microstructure at the interfacial

region, the nature of the fiber-matrix interface also affects the interfacial shear strengths. However, a comparison of the interfacial shear strengths of PC and PC + DS composites cannot be used to isolate the influence of matrix GBs and the nature of the fiber-matrix interface in determining the measured debond strengths, because both the number of interfacial GBs and the nature of the interfaces were different in the PC and the DS materials. However, a comparison of the DS (GB) and DS (GI) fibers shows that the matrix structure in the vicinity of the fiber can influence the measurements of interfacial shear strengths when the fiber-matrix interfaces are identical (the DS (GB) and DS (GI) fibers had undergone identical processing and possessed identical interfacial microstructures). From a mechanics perspective, the observed influence of matrix microstructure on the deformation and fracture behaviors during fiber pushout may manifest itself in a different stress state at the fiber-matrix interface. Thus, it might be argued that the GBs coincident at the fiber-matrix interface allow residual clamping stresses to be relieved, thereby requiring lower loads or shear stresses to cause interfacial debonding. Furthermore, the magnitude of thermal clamping stresses is expected to be larger in the DS composites, which were processed at appreciably higher temperatures compared to the PC composites. This would lead to an increased pushout load in the case of the DS composites as compared to the PC composites. Additional

work is necessary to examine the influence of processing temperatures/cooling rates on the thermal clamping contribution to the measurements of interfacial shear strengths. It is noteworthy, however, that limited thermal cycling (400 to 1100 K, 500 cycles in air) of the DS sapphire-NiAl composites did not impair the interfacial shear strength as measured using the fiber-pushout technique.[6]

B. Pushout Behavior: Influence of Specimen Bending

In thin discs ($t/h \leq 0.75$), the nucleation of back-face cracks during fiber pushout is further enhanced because of the specimen bending, which could start immediately after application of the load. This results in a compressive stress on the front face and tensile stress on the back face of the specimen. Cracks therefore nucleate along the radial GBs on the back face at low loads. In the case of thin PM specimens, where a large number of GBs are available, a continuous spectrum of loads, starting at very small loads, may lead to GB cracking on the back face of thin discs. This could lead to the unusual load vs displacement behavior presented in Figure 4(d) for thin PM specimens, where no sharp load drop is seen. This conjecture is further supported by the fact that a continuous AE signal activity without any major AE events (Figure 4(d)) accompanies fiber pushout in thin PM specimens. For the DS (GI) fibers in thin specimens, the crack nucleation is delayed until the tensile stress resulting from specimen bending exceeds the fiber-matrix interfacial strength. This results in higher mean values of τ_p for these fibers, about 80 MPa for thin DS (GI) and DS (GB) vs only 27 MPa for thin PM specimens. As expected, the apparent magnitude of the specimen bending (the combined influence of the GB cracks on the back face and the true elastic bending of the sample) is the largest in the thin PM specimens and smallest in the thin DS (GI) specimens, with the DS (GB) values lying in between.

Specimens with $t/h > 0.75$ to 1.0 were not affected to any significant level by bending, as indicated in Figure 9, which shows that the extent of pseudoelastic displacement measured at a constant load (1.37 N) is independent of specimen thickness. This observation is valid for all types of fibers examined in this study, $i.e.$, fibers in PM, DS (GB), and DS (GI), suggesting that the influence of the specimen bending is negligible for the ratio of the specimen thickness (t) to the grove width (h) larger than unity. This compares with the value of two for this ratio, estimated from a theoretical analysis.[11]

C. Zone DS Processing of Sapphire Fiber-NiAl Composites

Powder-cloth-processed sapphire-NiAl composite is not a suitable feedstock material for zone DS, because evidence of gaseous microporosities was observed at the fiber-matrix interface. The residues from the organic binders used in the PC processing presumably react with the NiAl melt and produce gaseous porosity at the fiber-matrix interface. This porosity, detrimental to the interfacial strength, would adversely affect the high-temperature strengthening expected from the sapphire

fibers. Such interfacial defects were absent in the DS specimens made from a cast sapphire-NiAl feedstock containing no binders.[6] These observations suggest that the as-cast sapphire-NiAl composites, prepared by the vacuum-melting and pressure-infiltration-casting techniques, would be an ideal feed material for the zone DS processing.

As demonstrated in the present study, the GBs anchored on the fiber-matrix interfaces in the PC specimens could be progressively eliminated by the DS process, thereby yielding large columnar NiAl grains that had completely engulfed the fibers. This indicates the potential of the DS process to create single-crystal NiAl matrix composites reinforced with sapphire fibers. The DS technique would also permit creation of dual-phase microstructures in the NiAl alloys, with fibers surrounded by an interlayer of a ductile second phase. This would permit exploitation of the improved room-temperature ductility advantages of microalloyed NiAl single crystals.[15] The significantly higher interfacial shear strengths of the single-crystal NiAl matrix composites would also permit achievement of the high-temperature creep strengthening due to the sapphire fibers, which has not yet been possible because of the poor interfacial strengths in PC processed composites.[4] The composite with a single-crystal matrix is also likely to have improved toughness because of the higher stresses required for the crack nucleation at the sapphire fiber-matrix interface. Finally, the contribution to the toughening resulting from the frictional shear stress would still operate in the single-crystal NiAl matrix composites, because the DS process did not affect the frictional shear stress.

V. CONCLUSIONS

The following conclusions can be drawn from this study on the deformation and fracture behavior during pushout testing of sapphire fibers in PC (PM) and PM + DS sapphire-NiAl composites.

1. The PC processed sapphire-NiAl composite is unsuitable as a feed material for the zone DS because of the formation of interfacial microporosity in the PM + DS material. Binder residues in the PC material may have caused these porosities to form, because no porosities were observed in the DS specimens that were made from a cast feedstock free of binders. The DS process resulted in progressive elimination of the matrix GBs initially anchored at the fiber-matrix interface.

2. The load-displacement behavior during the fiber-pushout test on sapphire-NiAl composites consists of an initial pseudoelastic response, followed by an inelastic response, and finally a frictional response, which accompanies the large scale, postdebond displacement of the fiber relative to the matrix. While the thick specimens ($t/h > 0.75$) showed an abrupt load drop at the maximum load, the PM and DS (GB) fibers in thin discs ($t/h \leq 0.75$) typically showed a continuous rather than an abrupt drop in the load after the maximum load was reached. The elastic bending of the test specimen during mechanical loading can be minimized at $t/h > 0.75$ to 1 for all types of

fibers; however, the DS (GI) fibers showed the smallest pseudoelastic deflections at all values of t/h ratios. A strong acoustic signal was generally associated with the stress τ_p.

3. In the thin PM specimens, the onset of the pseudoelastic response is associated with the nucleation of cracks on the NiAl GBs in contact with the sapphire fibers on both the front and back faces. For the PM fibers in thick discs ($t/h > 0.75$) and for the DS (GB) and DS (GI) fibers in both thick and thin test specimens, no front- or back-face cracks form at τ_p. The τ_p values are higher in the PM + DS composites than in the PM composites at all disc thicknesses. The highest τ_p values are observed for the fibers that are completely engulfed within the NiAl grains (DS (GI) fibers). The matrix GBs coincident at the fiber-matrix interface assist debonding at relatively low loads; hence, the measurements of interfacial shear strengths in a polycrystalline matrix may not reflect the inherent fiber-matrix bond strength.

4. In the inelastic regime, cracks nucleated on the back face of the test specimen traverse toward the front face, leading to complete fiber debonding at τ_m. The DS (GB) fibers show front-face cracking at GBs coincident on the fiber surface, and interfacial decohesion and GB cracking on the back face of the test specimen at τ_m. On the other hand, the DS (GI) fibers show limited interfacial decohesion and fine radial cracks on the back face but no damage on the front face at τ_m. The mean values of τ_m show a trend similar to τ_p, i.e., τ_m for DS (GI) > DS (GB) > PM. The frictional shear stress, τ_f, shows large scatter but appears to be independent of the specimen thickness, processing history, and matrix microstructure in the vicinity of the fiber.

5. As the sapphire fibers did not appear to pin the matrix GBs during DS, it is suggested that DS techniques can be used to fabricate sapphire-fiber-reinforced NiAl matrix composites with single-crystal matrices of controlled orientation. Finally, the DS process permits achievement of higher fiber-matrix interfacial shear strength compared to the current solid-state fabrication techniques.

REFERENCES

1. R.D. Noebe, R.R. Bowman, and J.I. Eldridge: *Intermetallic Matrix Composites*, Materials Research Society Symposia Proceedings, D.L. Anton, R. McMeeking, D. Miracle, and P. Martin, eds., Materials Research Society, Pittsburgh, PA, 1990, vol. 194, p. 323.
2. J.W. Pickens, R.D. Noebe, G.K. Watson, P.K. Brindley, and S.L. Draper: NASA TM 102060, NASA Lewis Research Center, Cleveland, OH, 1989.
3. A.K. Misra: NASA CR-191167, NASA Lewis Research Center, Cleveland, OH, July 1993.
4. R.R. Bowman: *Intermetallic Matrix Composites II*, Materials Research Society Symposia Proceedings, D.B. Miracle *et al.*, eds., Materials Research Society, Pittsburgh, PA, 1991, vol. 31 (10), p. 1172.
5. R.D. Noebe, A. Misra, and R. Gibala: *Iron Steel Inst. Jpn. Int.* 1991, vol. 31 (10), p. 1172.
6. S.N. Tewari, R. Asthana, and R.D. Noebe: *Metall. Trans. A*, 1993, vol. 24A, pp. 2119-25.
7. M.N. Kallas, D.A. Koss, H.T. Hahn, and J.R. Hellmann: *J. Mater. Sci.*, 1992, vol. 27 (14), p. 3821.
8. C.A. Moose, D.A. Koss, and J.R. Hellmann: *Intermetallic Matrix Composites*, Materials Research Society Symposia Proceedings, Materials Research Society, Pittsburgh, PA, 1990, vol. 194, p. 293.
9. D.B. Marshall: *Acta Metall. Mater.*, 1992, vol. 40, p. 427.
10. D.A. Koss, M.N. Kallas, J.R. Hellmann, J.M. Galbraith, and E.P. Rhyne: *HITEMP Rev. 1992*, NASA CP 10104, 25-1-25-12.
11. D.A. Koss, M.N. Kallas, and J.R. Hellmann: *Intermetallic Matrix Composites II*, Materials Research Society Symposia Proceedings, D.B. Miracle *et al.*, eds., Materials Research Society, Pittsburgh, PA, 1992, vol. 273, p. 303.
12. J.I. Eldridge and P.K. Brindley: *J. Mater. Sci. Lett.*, 1989, vol. 8, p. 1451.
13. J.I. Eldridge: NASA TM 105341, NASA Lewis Research Center, Cleveland, OH, 1991.
14. A.K. Misra: NASA CR-4171, NASA Lewis Research Center, Cleveland, OH, 1986.
15. J.E. Hack, J.M. Brezeski, and R. Darolia: *Scripta Metall.*, 1992, vol. 27, pp. 1259-63.